Particuology 8 (2010) 212–220

Contents lists available at ScienceDirect

Particuology

journal homepage: www.elsevier.com/locate/partic

Density functional theory study on the influence of cation ratio on the host layer structure of Zn/Al double hydroxides

Hong Yan [a], Min Wei [a,*], Jing Ma [b], Xue Duan [a]

[a] State Key Laboratory of Chemical Resource Engineering, Beijing University of Chemical Technology, Beijing 100029, China
[b] Institute of Theoretical and Computational Chemistry, Key Laboratory of Mesoscopic Chemistry of MOE, Nanjing University, Nanjing 210093, China

ARTICLE INFO

Article history:
Received 16 February 2009
Accepted 27 June 2009

Keywords:
Layered double hydroxide
Zn/Al molar ratio
Density functional calculation
Microstructure
Formation and bonding stability

ABSTRACT

A density functional theory (DFT) study has been carried out for $[Zn_{n-1}Al(OH_2)_{n+6}(OH)_{2n-2}]^{3+}$ ($n = 3$–6) and $[Zn_{n-1}Al(OH_2)_{2n-2}(OH)_{2n-2}]^{3+}$ ($n = 7$) clusters, which include the basic structural information of the brucite-like lattice structure of Zn/Al layered double hydroxides (LDHs) with Zn/Al molar ratio (R) in the range 2–6, in order to understand the effect of the Zn/Al ratio on the structure and stability of binary Zn/Al LDHs. Based on systematic calculations of the geometric parameters and formation energies of the cluster models, it was found that it is possible for Zn^{2+} and Al^{3+} cations to replace Mg^{2+} isomorphously in the brucite-like structure with different R values, resulting in differences in microstructure of the clusters and unit cell parameter a of the Zn/Al LDHs. Analysis of the geometry and bonding around the trivalent Al^{3+} or divalent Zn^{2+} cations reveals that Al^{3+} plays a more significant role than Zn^{2+} in determining the microstructure properties, formation and bonding stability of the corresponding Zn_RAl clusters when $R < 5$, while the influence of Zn^{2+} becomes the dominant factor in the case of $R \geq 5$. These findings are in good agreement with experiments. This work provides a detailed electronic-level understanding of how the composition of cations affects the microstructure and stability of Zn-containing binary LDH layers.

1. Introduction

Layered double hydroxides (LDHs), also known as hydrotalcite-like compounds or anionic clays, are a large group of both naturally occurring and synthetic intercalated materials with positively charged brucite-like metal hydroxide layers containing divalent and trivalent metal cations (Cavani, Trifirò, & Vaccari, 1991). The charge neutrality is ensured by interlayer anions that are easily exchangeable. The general formula of these compounds is $[M^{2+}_{1-x}M^{3+}_x(OH)_2]^{x+}(A^{n-}_{x/n})\cdot mH_2O$, where M^{2+} and M^{3+} are metal cations such as Mg^{2+}, Ni^{2+}, Mn^{2+}, or Zn^{2+} and Al^{3+}, Ga^{3+}, Fe^{3+} or Cr^{3+} that occupy octahedral positions in hydroxide layers; x is the molar ratio of the trivalent cation $M^{3+}/(M^{2+} + M^{3+})$, and A denotes interlayer charge-compensating anions (Duan & Evans, 2006; Rives, 2001). The wide choice of composition for both the metal cations and the interlayer anions gives rise to numerous LDH compositions, both purely inorganic or hybrid inorganic–organic phases. LDHs have received considerable attention due to their potential technological applications in the fields of catalysis (Sels, de Vos, & Jacobs, 2005), as gene and molecular reservoirs (Choy, Kwak, Park, Jeong, & Portier, 1999), optical materials (Itoh et al., 2005), functional hybrid nanostructured materials (Gursky et al., 2006), controlled drug-release systems (Mohanambe & Vasudevan, 2005), and films (Chen, Zhang, Fu, & Duan, 2006). Besides the best known Mg/Al LDHs, in recent years a great deal of attention has also focused on the development of Zn/Al hydrotalcite-like materials (Chang et al., 2005; Vial, Ghanbaja, & Forano, 2006), stemming from their potential applications such as nanocomposite materials (Cho, Jung, Jang, Oh, & Lee, 2008; Darder, López-Blanco, Aranda, Leroux, & Ruiz-Hitzky, 2005; Liu et al., 2006), polymer nanofillers (Illaik et al., 2008) and functional films (Yarger, Steinmiller, & Choi, 2008; Zhang et al., 2008).

The value of x, or the M^{2+}/M^{3+} ratio (R), plays an important role in the formation of the characteristic layered structure, since the charge density on the hydroxide layers of the LDH clearly depends on R. The anion-exchange capacity, and hence the number and arrangement of the charge-balancing anions in the LDH, may therefore be controlled by varying R (Cavani et al., 1991). It is often said (Duan & Evans, 2006) that pure LDH phases can only be formed for stoichiometries in the range $0.20 < x < 0.33$, i.e. M^{2+}/M^{3+} ratios in the range 2–4. For Zn/Al LDHs, however, it has been claimed that at neutral pH by using the coprecipitation method, LDH phases can be obtained with Zn/Al ratio varying from 5 to 1 (Barriga, Jones, Malet, Rives, & Ulibarri, 1998; Rojas, de Pauli, Barriga, & Avena, 2008).

* Corresponding author. Tel.: +86 10 64412131; fax: +86 10 64425385.
E-mail address: weimin@mail.buct.edu.cn (M. Wei).

1674-2001/$ – see front matter © 2010 Chinese Society of Particuology and Institute of Process Engineering, Chinese Academy of Sciences. Published by Elsevier B.V. All rights reserved.
doi:10.1016/j.partic.2010.03.004

Nomenclature

R	Zn^{2+}/Al^{3+} molar ratio
ΔE_f	calculated formation energy (kcal/mol)
E	calculated total energy (kcal/mol)

Understanding the properties and exploiting the chemistry of LDHs require a detailed knowledge of the structure. However, because of the inherently structural disorder and generally low crystallinity of LDHs, the determination of the complete LDH structure with different M^{2+}/M^{3+} ratios by X-ray diffraction is rarely possible. With recent advances in computational software and hardware, theoretical calculations are now capable of extending the scope of study of these materials beyond experimental observations. A number of force-field based simulations (Aicken, Bell, Coveney, & Jones, 1997; Greenwell, Jones, Coveney, & Stackhouse, 2006; Hou, Kalinichev, & Kirkpatrick, 2002; Li et al., 2006; Lombardo, Pappalardo, Costantino, Costantino, & Sisani, 2008; Lombardo et al., 2005; Thyveetil, Coveney, Greenwell, & Suter, 2008) and quantum chemical calculations (Greenwell, Stackhouse, Coveney, & Jones, 2003; Pu & Zhang, 2005; Refson, Park, & Sposito, 2003; Sainz-Diaz, Timon, Botella, & Hernandez-Laguna, 2000; Sato et al., 2003; Trave, Selloni, Goursot, Tichit, & Weber, 2002) have been reported for the study of some specific properties related to the interlayer anions and the electronic structure inside the LDH host layers.

In our previous theoretical work (Yan et al., 2008), the template-directed method was extended to the formation of LDH layers by using a series of cluster models, and further study has been carried out for the understanding of structural properties and relative stability of LDHs layer containing different divalent cations (Yan et al., 2009). This finite cluster approach has been used many times in clay chemistry as has been documented in several reviews (Sauer, 1989; Sauer, Ugliengo, Garonne, & Saunders, 1994), since it could handle accurate quantum computations for systematic energies and cluster structures.

In this work, the structural properties and stability of a series of Zn_R–Al clusters (R = 2–6) are studied in order to understand of the influence of the Zn/Al ratio on the structures and stability of the Zn/Al LDH layers. A series of clusters with formulae $[Zn_{n-1}Al(OH_2)_{n+6}(OH)_{2n-2}]^{3+}$ (n = 3–6, corresponding to R = 2–5) and $[Zn_{n-1}Al(OH_2)_{2n-2}(OH)_{2n-2}]^{3+}$ (n = 7, corresponding to R = 6), based on the characteristic octahedrally coordinated metal cations found in LDH layers, have been employed in the density functional theoretical study. These models are derived from our previous cluster models ($[Mg_n(OH_2)_{n+6}(OH)_{2n-2}]^{2+}$ (n = 2–6)) for the formation of brucite (Yan et al., 2008), by first substituting the Mg^{2+} cations by Zn^{2+} and subsequently replacing one of them by an Al^{3+} ion. As a result, the cluster models can represent the ordered microstructure of the Zn/Al LDH layers with Zn/Al ratio R in the range 2–6 with the most economical size. In this paper, the geometric parameters (bond lengths, interatomic distances and bond angles) and formation energy of the cluster models are systematically discussed.

2. Computational details

In order to carry out the theoretical study, it is necessary to choose an economical cluster model which includes the basic structural information. As referred to above, in the present work, the $[Zn_{n-1}Al(OH_2)_{n+6}(OH)_{2n-2}]^{3+}$ (n = 3–6) and $[Zn_{n-1}Al(OH_2)_{2n-2}(OH)_{2n-2}]^{3+}$ (n = 7) clusters are proposed to be the most practical model for understanding the Zn/Al LDH layers with Zn/Al ratio in the range 2–6. As shown in Fig. 1, in these models, each bridging oxygen atom in the M–O–M angles is set to be bonded to one hydrogen atom (OH group), and the terminal oxygen atoms are set to be bonded to two hydrogen atoms (OH_2 group), to avoid the presence of unpaired electrons in the truncated ligands. Thus each model includes $2(n-1)$ OH groups at bridging positions and $(n+6)$ OH_2 groups at terminal edges, except for

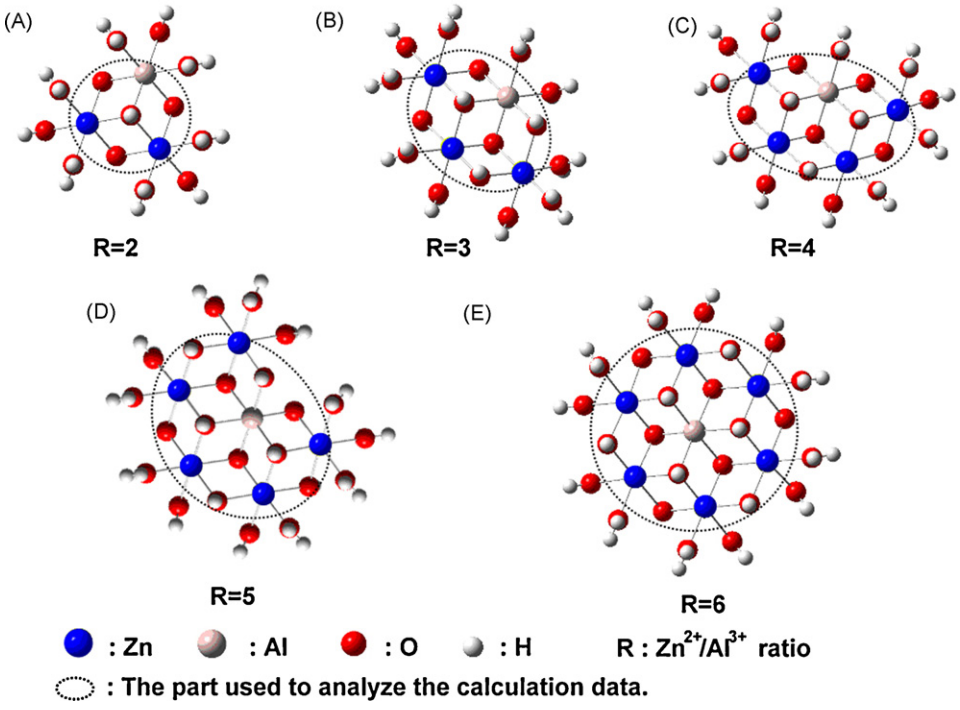

Fig. 1. Computational models of (A)–(D) $[Zn_{n-1}Al(OH_2)_{n+6}(OH)_{2n-2}]^{3+}$ (n = 3–6) and (E) $[Zn_{n-1}Al(OH_2)_{2n-2}(OH)_{2n-2}]^{3+}$ (n = 7) clusters with Zn/Al ratios (R) in the range 2–6. The parts used to analyze the calculation results are circled by dots.

the $[Zn_{n-1}Al(OH_2)_{2n-2}(OH)_{2n-2}]^{3+}$ ($n=7$) cluster (Fig. 1(E)). These models are representative of the structure of the Zn/Al LDH crystal lattice since the results from XANES spectroscopy show that the Zn^{2+} cation maintains an octahedral environment in the brucite-like layers, even though it is known to have some tendency to be tetrahedrally coordinated in other materials (del Arco, Rives, Trujillano, & Malet, 1996).

Theoretical calculations were carried out on the $[Zn_{n-1}Al(OH_2)_{n+6}(OH)_{2n-2}]^{3+}$ ($n=3$–6) and $[Zn_{n-1}Al(OH_2)_{2n-2}(OH)_{2n-2}]^{3+}$ ($n=7$) clusters (abbreviated hereafter as Zn_R–Al). The geometrical optimization for the cluster models was performed by density functional theory (DFT) with the three-parameter hybrid functional (B3LYP) (Becke, 1988, 1993; Lee, Yang, & Parr, 1988). The effective core potential (ECP), LANL2DZ (Hay & Wadt, 1985a, 1985b; Wadt & Hay, 1985), and the full electron basis sets, 6-31G(d) (Petersson & Al-Laham, 1991), were employed for the metal ions and OH_2 ligands, respectively. The calculations were performed with the Gaussian 03 program suite (Frisch et al., 2003). No constraints were imposed on the geometry in any of the computations. The attainment of the energy minimum of the structure in the full geometry optimization was tested by frequency calculations when $R=2$ and 3 (i.e. $n=3$ and 4). The reported energies were also corrected for zero-point energy (ZPE) when $R=2$ and 3.

3. Results and discussion

3.1. Geometry of the models

The optimized structures of the Zn_R–Al ($R=2$–6) clusters with different Zn/Al ratios display different geometries with C1 symmetry. In the following discussion, we concentrate on the parts of the cluster which are linked around the bridging OH groups and are circled by dots in Fig. 1. The optimized geometries of the calculated clusters such as average bond lengths, interatomic distances and bond angles are listed in Table 1, along with the experimental data for LDHs.

Fig. 1 and Table 1 show that the general geometry of the calculated Zn_R–Al ($R=2$–6) clusters is close to that of the octahedral

Table 1
Optimized geometries of the Zn_R–Al clusters for the Zn/Al ratio (R) in the range 2–6 along with the experimental results.

R[a]	Zn–O	Al–O	Me–O[b]		∠OZnO	∠OAlO	∠OMeO[c]	
	Calc.	Calc.	Calc.	Exptl.	Calc.	Calc.	Calc.	Exptl.
(A) Average metal–oxygen bond lengths (in nm), and metal–oxygen–metal bond angles (in degrees)								
2	0.2103	0.1851	0.2019	0.2070[d] 0.2015[d] 0.2268[e,f]	75.10	86.39	78.86	86.43[e,f]
3	0.2111	0.1885	0.2047		76.70	86.04	79.84	
4	0.2113	0.1908	0.2062		77.88	84.73	79.50	
5	0.2123	0.1928	0.2074		78.01	86.08	80.56	
6	0.2122	0.1929	0.2083		78.75	85.02	80.32	

R[a]	Zn···Zn	Zn···Al	Me···Me[g]		O···O_{ZnZn}[h]	O···O_{ZnAl}[i]	O···O_{MeMe}[j]	
	Calc.	Calc.	Calc.	Exptl.	Calc.	Calc.	Calc.	Exptl.
(B) Average interatomic distances (in nm)								
2	0.3171	0.3105	0.3127	0.3010[k,l] 0.3060[k,m,n] 0.3076[k,o] 0.3080[k,p] 0.3085[q] 0.3194[e,f]	0.2730	0.2535	0.2600	2.622[c]
3	0.3221	0.3123	0.3162	0.3030[k,l] 0.3086[k,r] 0.3090[k,p]	0.2726	0.2581	0.2639	
4	0.3218	0.3132	0.3169	0.3060[k,l] 0.3080[k,m] 0.3100[k,p]	0.2746	0.2584	0.2653	
5	0.3222	0.3147	0.3180	0.3100[k,m]	0.2737	0.2626	0.2675	
6	0.3196	0.3184	0.3190		0.2779	0.2604	0.2691	

[a] Zn^{2+}/Al^{3+} ratio (R).
[b] Average metal–oxygen bond length of Zn–O and Al–O: Me–O = m(Zn–O) + n(Al–O)/($m+n$), m and n are the number of the Zn–O and Al–O bonds in the Zn_R–Al clusters, respectively.
[c] Average metal–oxygen–metal bond angle of ∠OZnO and ∠OAlO, calculated as in Note b.
[d] Reference: Lombardo et al. (2005).
[e] Data for the metal hydroxide.
[f] Reference: Oswald and Asper (1977).
[g] Average metal–metal interatomic distance of Zn···Zn and Zn···Al, calculated as in Note b.
[h] Average O···O distance across Zn···Zn.
[i] Average O···O distance across Zn···Al.
[j] Average O···O distance of O···O_{ZnZn} and O···O_{ZnAl}, calculated as in Note b.
[k] Unit cell parameter a.
[l] Reference: Seftel et al. (2008).
[m] Reference: Delgado, De Pauli, Carrasco, and Avena (2008).
[n] Reference: Jaubertie, Holgado, Román, and Rives (2006).
[o] Reference: Pisson, Morel, Morel-Desrosiers, Taviot-Guého, and Malfreyt (2008).
[p] Reference: Barriga et al. (1998).
[q] Reference: Ennadi, Legrouri, de Roy, and Besse (2000b).
[r] Reference: Prevot, Forano, Besse, & Abraham (1998).

layer of LDHs. The local geometries around the metal cations are distorted away from that of brucite ($Mg(OH)_2$) as a result of the substitution of Mg^{2+} by Zn^{2+} and Al^{3+}. This leads to a decrease in the average metal–oxygen distance Me–O (0.2019–0.2083 nm), Me···Me (0.3127–0.3190 nm) and O···O_{MeMe} (0.2600–0.2691 nm) distance compared with the corresponding values in brucite (0.2102 nm, 0.3142 nm, and 0.2787 nm for Mg–O, Mg···Mg and O···O, respectively) (Zigan & Rothbauer, 1967), with the average O–Me–O bond angles (78.86–80.32°) being less distorted than those in brucite (83.30°). This result is consistent with the experimental findings that the bond lengths, interatomic distance and bond angles for LDH are all smaller than the corresponding values for brucite (Rives, 2001).

Good agreement was found between the theoretically calculated geometric parameters and the experimental values. The calculated Me–O bond lengths, O···O_{MeMe} distances and O–Me–O bond angles are slightly shorter than the corresponding experimental ones, while the average Me···Me distances are slightly longer than the experimental values. This may be due to the fact that the experimental values are derived from crystal data for LDHs, in which both the interactions between adjacent layers and the interaction between layers and interlayer anions are present. Indeed, the experimental Me···Me distances vary for Zn/Al LDHs with the same R due to the different anions present. However, the calculated clusters only include the basic information about a single layer. On the other hand, the experimental crystal data obtained by diffraction techniques can only give the average values of parameters for Zn/Al LDH, since Zn and Al have effectively identical scattering power, making them indistinguishable by X-ray diffraction (Ennadi, Legrouri, de Roy, & Besse, 2000a). In this work, the cation arrangement is fixed; this allows us to obtain a detail understanding of the geometries around Zn^{2+} or Al^{3+} individually. Therefore, it is possible to investigate which cation plays a more significant role in determining the structural properties of the Zn_R–Al (R = 2–6) clusters with different Zn/Al ratios.

3.1.1. Bond length, bond strength and bond angle

Fig. 2(A) illustrates the average bond lengths of the Zn_R–Al (R = 2–6) clusters as a function of the Zn/Al ratio (R). All the Zn–O (line (a)), Al–O (line (b)) and Me–O distances (line (c)) increase with increasing R (decreasing Al content). For the same R value, the Zn–O distance is significantly longer than Al–O as a consequence of the smaller ionic radius of Al^{3+}, 0.0535 nm, as compared to that of Zn^{2+}, 0.0740 nm (Shannon, 1976). The Al–O distance increases gradually when R < 5, while maintaining a nearly constant value from R = 5 to R = 6. On the other hand, the increase of the Zn–O distance with R is much more uniform than that of the Al–O distance. Comparing lines (a) and (b) with line (c) shows that the average metal–oxygen bond length (Me–O) is influenced more significantly by Al–O, since the variation of Me–O is closer to that of Al–O. This indicates that the trivalent Al^{3+} cation plays a more significant role than the divalent Zn^{2+} cation in determining the average bond length (Me–O) of the Zn_R–Al cluster, especially when R < 5.

It is known that shorter bond lengths result in stronger bonds. Consequently, it is possible for us to analyze the bond strengths in the Zn_R–Al clusters by monitoring the relationship between the average metal–oxygen bond length and R. Fig. 2(A) shows that the metal–oxygen bond strength becomes weaker with increasing R. In other words, the bonding around the cations should become more stable with decreasing R. This may imply that the pure Zn/Al LDH exists at relatively low R values. It can also be found from Fig. 2(A) that the bond strength of Zn–O is nearly constant from R = 2 to 6, while Al–O rapidly becomes weaker with increasing R. These results show that the Al–O distance dominates the bonding stability of the corresponding clusters, especially when R < 5.

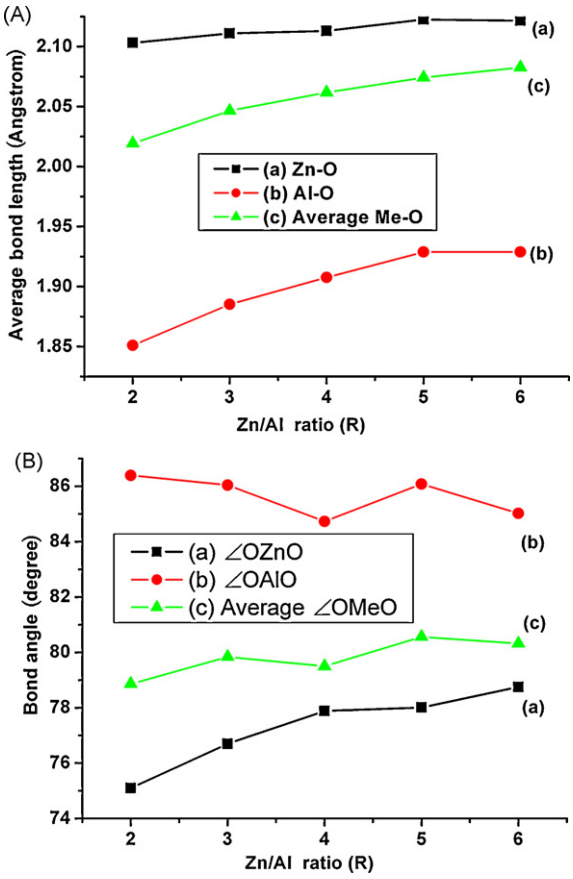

Fig. 2. (A) Average metal–oxygen bond lengths and (B) oxygen–metal–oxygen bond angles of the Zn_R–Al (R = 2–6) clusters as a function of the Zn/Al ratio (R).

The average oxygen–metal–oxygen bond angles of the Zn_R–Al (R = 2–6) clusters, which indicate the distortion of the octahedral layers, are displayed as a function of R in Fig. 2(B). The O–Zn–O bond angles (line (a)) monotonically increase with increasing R. However, the O–Al–O bond angle (line (b)) fluctuates with increasing R with a minimum at R = 4. The O–Zn–O angle is smaller than the O–Al–O angle, suggesting the opposite relationship between the bond length and bond angle. Similar to the O–Al–O angle, the average O–Me–O angle fluctuates with increasing R, showing an inflection at R = 4, thus indicating that the trivalent Al^{3+} cations make the major contribution to determining the oxygen–metal–oxygen bond angle in Zn_R–Al clusters.

3.1.2. Interatomic distances

The average metal–metal interatomic distances of the Zn_R–Al (R = 2–6) clusters as a function of the Zn/Al ratio (R) are shown in Fig. 3(A). It is known that the average distance between two closest metal cations in the brucite-like layers is equivalent to the unit cell parameter a of LDH crystals (Cavani et al., 1991). Therefore, the analysis of metal–metal interatomic distances is helpful in understanding the structure of the corresponding LDHs. As displayed in Fig. 3(A), the Zn···Zn distance (line (a)) is larger than the Zn···Al distance (line (b)) for the same R. The Zn···Al distance increases with increasing R, and the variation is more dramatic from R = 5 to 6 than from R = 2 to 5. However, the variation of the Zn···Zn distance is different from that of Zn···Al, rising sharply to a maximum from R = 2 to 3 and then remaining nearly constant from R = 3 to 5, and then decreasing sharply from R = 5 to 6. The average metal–metal interatomic distance Me···Me increases gradually with R from 2 to 6, showing a similar upward trend to that of Zn···Al. This trend is

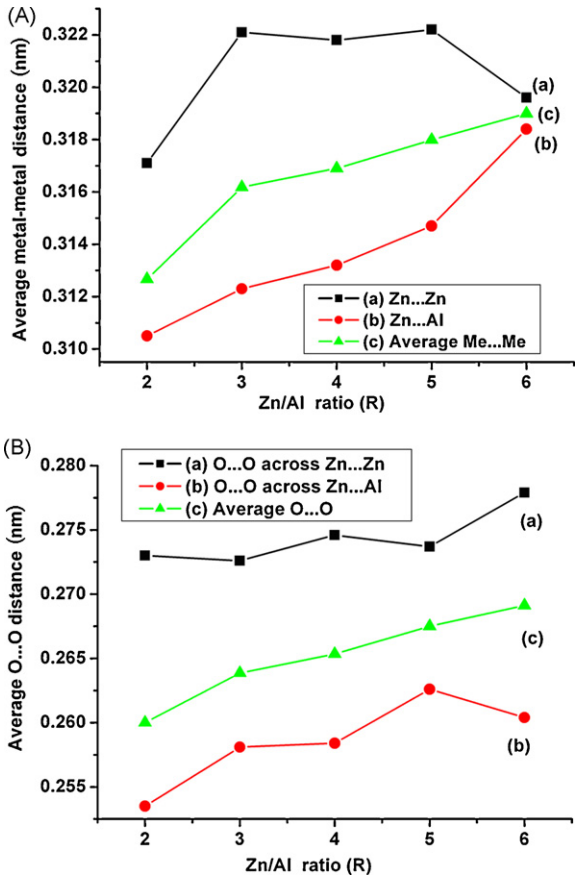

Fig. 3. (A) Average metal–metal and (B) oxygen–oxygen interatomic distances of the Zn_R–Al (R = 2–6) clusters as a function of the Zn/Al ratio (R).

in accordance with reports that for samples prepared by coprecipitation, the a dimension of the unit cell steadily increased as the Zn/Al ratio was increased (Barriga et al., 1998; Bonnet et al., 1996; Rojas et al., 2008; Seftel et al., 2008). This finding reveals that the geometry around Al^{3+} plays a more important part in determining the Me···Me distance, i.e. the unit cell parameter a. It is to be noted that the changes in Me···Me distance from R = 3 to 6 are less evident than that from R = 2 to 3. When R = 6, the Me···Me distances (0.3190 nm) are very close to that of $Zn(OH)_2$ (0.3194 nm), suggesting that when the Al^{3+} content decreases sufficiently, the Zn^{2+} cations become the dominant factor influencing the Zn_n–Al cluster, leading to a structure similar to that of $Zn(OH)_2$. This can account for the experimental fact that pure LDHs were obtained only for Zn/Al ratios of 1–5; larger values lead to coprecipitation of zinc-containing impurities (ZnO and $Zn(OH)_2$) (Barriga et al., 1998; Bonnet et al.,1996; Yarger et al., 2008).

The O···O distance is also closely related to the distortion of the LDH layers. The flattening of the octahedra brings about short O···O distances in the shared octahedral edges, as shown in Fig. 3(B). The O···O distance across Zn···Zn (line (a)) fluctuates with R, while the O···O distance across Zn···Al (line (b)) increases from R = 2 to 5, and then decreases from R = 5 to 6. The O···O distance across Zn···Zn is larger than that across Zn···Al for the same value of R. On the other hand, the average O···O distance ($O\cdots O_{MeMe}$, line (c)) increases gradually with increasing R. This suggests that the trivalent cation plays a more significant role in determining the $O\cdots O_{MeMe}$ distance, especially when R < 5, since $O\cdots O_{MeMe}$ displays an upward trend from R = 5 to 6, which is similar to that of the O···O distance across Zn···Zn but opposite to the trend for the O···O distance across Zn···Al.

Based on the above discussion, it can be concluded that the trivalent Al^{3+} cation plays a more significant role than the divalent Zn^{2+} cation in determining the microstructure parameters of the calculated Zn_R–Al clusters especially when R < 5. This agrees well with the experimental observation that Zn/Al LDH phases can be obtained with Zn/Al ratios varying from 5 to 1 (Barriga et al., 1998; Rojas et al., 2008).

3.2. Formation energy

In order to investigate the influence of the Zn content on the formation of the clusters, the formation energy was calculated as the energy difference of the following reactions:

$$[Zn_{n-2}Al(OH_2)_{n+5}(OH)_{2n-4}]^{3+} + [Zn(OH_2)_6]^{2+} + 2OH^- \rightarrow [Zn_{n-1}Al(OH_2)_{n+6}(OH)_{2n-2}]^{3+} + 5H_2O \quad (n = 3\text{–}6), \tag{1}$$

and

$$[Zn_{n-2}Al(OH_2)_{n+5}(OH)_{2n-4}]^{3+} + [Zn(OH_2)_6]^{2+} + 2OH^- \rightarrow [Zn_{n-1}Al(OH_2)_{2n-2}(OH)_{2n-2}]^{3+} + 6H_2O \quad (n = 7). \tag{2}$$

The formation energy of the $[Zn_{n-1}Al(OH_2)_{n+6}(OH)_{2n-2}]^{3+}$ (n = 3–6) and $[Zn_{n-1}Al(OH_2)_{2n-2}(OH)_{2n-2}]^{3+}$ (n = 7) clusters can be obtained based on the equation:

$$\Delta E_f = E(\text{product}) - E(\text{reactant}), \tag{3}$$

where ΔE_f denotes the formation energy of the Zn_R–Al (R = 2–6) clusters, and E(product) and E(reactant) denote the optimized total energy of the products and reactants, respectively, in Eq. (1) or (2). The formation energies and total energies of the calculated Zn_R–Al clusters are listed in Table 2. The values $E_{H_2O} = -76.4090$ a.u., $E_{H_2O}(ZPE) = -76.3878$ a.u. computed with 6-31G(d) basis sets (1 a.u. = 627.51 kcal/mol), and $E_{[Zn(OH_2)_6]^{2+}} = -523.5$ a.u., which represents the total energy of the $[Zn(OH_2)_6]^{2+}$ cluster, are adopted from our previous computations (Yan et al., 2008).

Fig. 4 illustrates the dependence of the formation energy of the Zn_R–Al clusters on the Zn/Al ratio (R). It can be seen that the formation energy changes only very slightly from R = 3 to 5 with an inflection when R = 4, while the increase is very obvious when R increases from 5 to 6. This indicates that the formation of the Zn_R–Al cluster from R = 3 to 5 is much more favorable than for R = 5 to 6. The formation energy of the Zn_R–Al clusters is similar when R is between 3 and 5. This also suggests that as the cluster size becomes larger and the Zn content becomes higher, the structure of the cluster becomes closer to $Zn(OH)_2$ and formation of the pure ZnAl-LDH phase becomes more difficult to sustain. The finding is also consistent with experiment, since it has been reported that low values of x lead to a high density of Zn octahedra in the brucite-like sheets, acting as nuclei for the formation of $Zn(OH)_2$ (Barriga et al., 1998; Seftel et al., 2008).

Table 2
Calculated formation energies (ΔE_f) and total energies (E) of the Zn_R–Al (R = 2–6) clusters in kcal/mol.

R[a]	ΔE_f	E
2		−1364.0[b]
3	−1256.7	−1657.8[b]
4	−1249.1	−1951.9
5	−1254.9	−2245.7
6	−1213.3	−4951.1

[a] Zn/Al ratio (R).
[b] With ZPE correction.

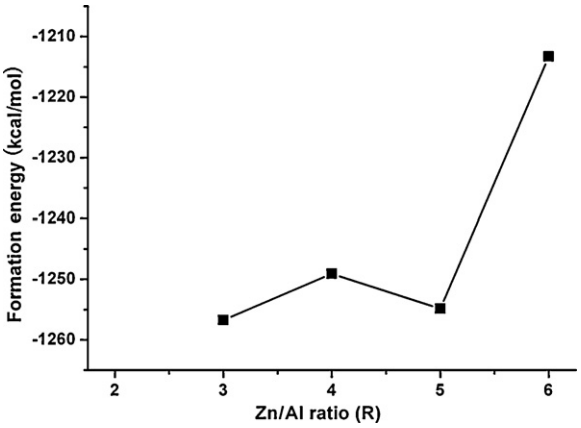

Fig. 4. The relationship between the formation energy ΔE_f of the Zn_R–Al (R = 3–6) clusters and the Zn/Al ratio (R).

4. Conclusions

A series of density functional calculations for $[Zn_{n-1}Al(OH_2)_{n+6}(OH)_{2n-2}]^{3+}$ (n = 3–6) and $[Zn_{n-1}Al(OH_2)_{2n-2}(OH)_{2n-2}]^{3+}$ (n = 7) clusters have been performed at DFT/UB3LYP level, for the purpose of understanding the effect of varying Zn/Al ratios (R) on the structure and stability of Zn/Al binary LDH layers.

The cluster models employed in this work include the basic information about the lattice structure of the Zn/Al LDH host layers while having the most economical size, with Zn/Al ratios in the range 2–6, and have succeeded in delineating the influences of the Zn/Al ratio on the structural properties and formation and bonding stability of the corresponding Zn/Al LDHs.

It was found that both Zn^{2+} and Al^{3+} can isomorphically substitute Mg^{2+} in the hydrotalcite-like structure. The formation or bonding stability of the corresponding Zn_R–Al (R = 2–6) clusters decreases with increasing R. Different R values result in different microstructures of the clusters, and thus influence the variation of the unit cell parameter a of the LDH crystal. By analyzing the structural and bond properties of the Zn^{2+} and Al^{3+} cations separately, their individual contributions to the whole cluster is clearly presented. The trivalent Al^{3+} cation plays a more significant role than the divalent Zn^{2+} cation in determining the microstructure properties, formation and bonding stability of the corresponding Zn_R–Al (R = 2–6) clusters, especially when $R < 5$. When $R \geq 5$, the Zn^{2+} cations occupy most of the cation sites of the cluster and the structure is closer to that of $Zn(OH)_2$. These findings agree well with experimental results.

Acknowledgements

This work was supported by the National Natural Science Foundation of China and the Program for Changjiang Scholars and Innovative Research Teams in Universities (Grant No. IRT0406).

Appendix A.

Cartesian coordinates of optimized models

(1) $[Zn_2Al(OH_2)_9(OH)_4]^{3+}$
O, 0, −3.4177256869, 0.7172230949, 1.8359532436
H, 0, −3.4109338243, 0.7228568909, 2.8085634067
Zn, 0, −1.7357323788, 0.7103223843, 0.5309939188
O, 0, −3.2726208651, −0.7136142843, −2.8645831706
H, 0, −3.4162563721, −0.4857463636, −3.8033333435
Zn, 0, 1.3755879652, 0.8682510212, 1.1205174295
O, 0, 2.4457113248, 0.9516480761, 2.9591832886
H, 0, 2.0811495608, 1.0090077006, 3.8589616457
O, 0, 0.1877447117, 0.4486775073, −0.7646991548
H, 0, 0.2586924819, 0.9647899836, −1.5790945314
O, 0, 0.3455087838, −3.422478047, −0.5690988829
H, 0, 0.713749346, −3.9607918082, 0.1545956084
O, 0, 2.9640775649, 1.7858232217, 0.163602255
H, 0, 3.399314844, 1.3681619866, −0.6184863473
O, 0, 3.9120747886, 0.1967452769, −1.9031352783
H, 0, 4.0919630747, 0.6042059935, −2.772186118
O, 0, −0.3811310938, 1.5663524867, 1.6579153168
H, 0, −0.5563583085, 2.1875300134, 2.3779150947
Al, 0, 0.2152527437, −1.4014384213, −0.6472975225
O, 0, 1.3677367163, −1.1586443161, 0.7768249985
H, 0, 1.5036595945, −1.7509871855, 1.5292214911
O, 0, −0.778407495, −1.8127572292, −2.3340492584
H, 0, −0.2958713691, −1.7692020297, −3.1781615866
O, 0, −1.4373909819, −1.2751933556, 0.1780406788
H, 0, −1.7998185878, −1.9402516469, 0.7802189744
O, 0, 1.7633461911, −1.5702397678, −1.9448122395
H, 0, 2.1548987184, −2.4592082009, −2.0179653361
O, 0, −2.9265517865, 1.3543227941, −1.033527674
H, 0, −3.1704898745, 0.7350908684, −1.7637189594
H, 0, −0.3033137261, −3.9667989367, −1.052475604
H, 0, −4.3344266178, 0.8922547526, 1.5623050608
H, 0, 3.404715569, 1.0948762012, 3.0360880025
H, 0, 2.5214841698, −0.9263658956, −1.9024516276
H, 0, 4.7596487198, −0.2140253587, −1.6453078729
H, 0, 3.2032904728, 2.7276147906, 0.1954380301
H, 0, −3.2423513895, 2.2479863731, −1.2483027402
H, 0, −4.0308080865, −1.2835661632, −2.6338733248
H, 0, −1.7048690311, −1.4788583155, −2.4793355594

(2) $[Zn_3Al(OH_2)_{10}(OH)_6]^{3+}$
O, 0, −2.9792919607, −1.1903317995, 1.5691211877
H, 0, −3.3345022879, −1.9172195111, 2.1080509003
Zn, 0, −1.4511036893, −1.0554971346, −0.0027269611
O, 0, −2.2926536516, −2.4526869314, −1.5184140194
H, 0, −2.9122735658, −2.2384125518, −2.2361233612
O, 0, 1.9655226348, 2.2636058139, 1.312460726
H, 0, 2.5872623398, 2.0615496432, 2.0306677689
O, 0, 0.5635258516, −0.5907021119, −0.9878913598
H, 0, 0.5669136294, −0.4616448767, −1.947980476
O, 0, 2.9648422579, −3.4719947312, 1.1214057252
H, 0, 3.236041035, −3.4610182835, 2.055485449
O, 0, 0.3631636614, 2.251157768, −0.8175362877
H, 0, 0.7106893048, 2.5455777985, −1.6709461453
O, 0, 2.7798958281, 1.0001572261, −1.0573902684
H, 0, 3.4315865754, 1.6947918962, −0.8581343032
Zn, 0, 1.5632979965, −2.1744143541, 0.0705936123
O, 0, 2.06289016, −0.4457580325, 1.1166291218
H, 0, 1.9024536429, −0.4800435199, 2.0703895382
O, 0, 1.2749056802, −3.987986643, −1.0906830336
H, 0, 1.3664497067, −4.2921796879, −2.009517571
O, 0, −0.3332471584, −2.6254875273, 0.6436567801
H, 0, −0.5068417129, −2.978449878, 1.5286105109
O, 0, 3.52843563, −1.6756835512, −1.1159510026
H, 0, 3.7660816058, −2.0421939507, −1.9876973821
H, 0, 2.9164453244, −4.4081208165, 0.8567959431
H, 0, −3.7331429806, −0.6285806948, 1.3208057539
H, 0, 1.5314270428, 3.1387958114, 1.4845267269
H, 0, 4.2347390244, −1.9696216162, −0.5096792048
H, 0, 3.259271641, 0.1375964727, −1.1166788103
H, 0, −2.5426351261, −3.339020302, −1.2075663432
H, 0, 0.3504166911, −4.144144796, −0.8161093095
O, 0, −1.8870189913, 3.6866776145, 1.0295357563
O, 0, −2.5779908405, 0.4869310369, −0.7095333069
O, 0, −0.5157803256, 0.7318757876, 1.0048626512
O, 0, −2.4838985951, 3.498281092, −1.780600541
H, 0, −1.0827412142, 4.1035679508, 1.4241566971
H, 0, −2.6369963531, 3.8267880571, 1.6308421555
H, 0, −3.241773686, 0.4288510749, −1.4099499986

Appendix A (*Continued*)

H, 0, −0.615865925, 0.7769866612, 1.9659122869
H, 0, −2.7806647585, 3.3719777626, −2.6972715694
H, 0, −2.7399191761, 4.3996472422, −1.5223902377
O, 0, 0.607046484, 4.6367746674, 1.8635186417
H, 0, 0.7002654883, 4.9852964534, 2.7702930795
H, 0, 0.8792070602, 5.3750763179, 1.2867100595
Zn, 0, −1.5995427251, 2.1457789195, −0.3619517325
Al, 0, 1.1527527612, 0.8553451536, 0.1241403167

(3) $[Zn_4Al(OH_2)_{11}(OH)_8]^{3+}$
O, 0, −1.891412981, −0.7216942777, 3.1965572706
H, 0, −2.1251595885, −1.0046056543, 4.0956290602
Zn, 0, −0.2652514142, −1.4107063837, 1.8837432826
O, 0, 0.030640263, −3.4580797356, 2.6542836517
H, 0, −0.6010014212, −4.187359895, 2.53972988
O, 0, 1.4002912851, −0.9281333589, 0.4177990664
H, 0, 1.7263573681, −1.5923771582, −0.2061475908
O, 0, 4.0765856635, 1.0616615118, 3.1502757692
H, 0, 3.9426402061, 1.8778577979, 3.6619264589
O, 0, 2.2710506378, 0.625830465, −1.6162808661
H, 0, 3.1316494828, 0.7636687912, −1.1639402912
Zn, 0, 2.6526583298, −0.0527651797, 1.9245958915
O, 0, 1.8002866207, 1.5363758524, 0.9657412225
H, 0, 1.5605700977, 2.3809319189, 1.3683244534
O, 0, 3.7607601143, −1.7028656266, 2.8546414593
H, 0, 4.2168791533, −2.5181392802, 2.5868808804
O, 0, 1.2475708274, −0.8794611436, 3.1652137472
H, 0, 0.9601071599, −0.3776746815, 3.9431298994
O, 0, 4.3294338858, 0.2858799377, 0.3344094625
H, 0, 5.0235208316, −0.3656220142, 0.1265508413
H, 0, 4.6072903249, 0.4660945187, 3.7095075695
H, 0, −2.7279314519, −0.6527245332, 2.6841566296
H, 0, 4.8040395571, 1.0573583107, 0.6962542475
H, 0, 2.1677290096, 1.2586979012, −2.3553821583
H, 0, 0.4003131828, −3.5518313566, 3.5475402919
H, 0, 2.962034158, −1.9543128161, 3.3669792225
O, 0, −3.6884324901, −0.9566738715, 1.0823290133
O, 0, −1.5580836924, −2.2439824922, 0.4939946653
O, 0, −0.8320970654, 0.383835466, 0.7583415184
O, 0, −3.1956279437, −1.9882468909, −2.0843069351
H, 0, −4.655226342, −1.0646690634, 1.0871941185
H, 0, −3.2674466512, −1.8520650951, 1.0471182482
H, 0, −1.3031659945, −3.0875297342, 0.0938421874
H, 0, −1.192249811, 1.1265800167, 1.2650095491
H, 0, −3.2556650479, −2.9581262104, −2.0984737372
H, 0, −4.0369152859, −1.6561788687, −2.4389747081
Zn, 0, −2.1062269154, −0.6465743578, −0.6848031343
Zn, 0, −1.1057611921, 1.664179963, −2.6330965405
O, 0, −2.8389822674, 0.8764372487, −1.8142326761
O, 0, −0.2875067929, −0.1427517318, −1.7518014522
O, 0, 0.0762862263, 2.2925748482, −1.1098948723
O, 0, −2.2467570962, 1.0428052069, −4.3974087298
O, 0, −1.5938221395, 3.6025543496, −3.485329593
H, 0, −3.4837559668, 1.4716014739, −1.4027957139
H, 0, 0.2018300739, −0.7817947249, −2.2897799767
H, 0, 0.2079417417, 3.1702997659, −0.7312973967
H, 0, −2.1540790283, 0.4340619953, −5.149124962
H, 0, −2.9704655873, 0.712440303, −3.8220046402
H, 0, −1.84476617, 4.4259672223, −3.0327960812
H, 0, −2.1726878828, 3.5242924605, −4.2648487489
H, 0, 0.9637608811, 1.4636058769, −4.758324287
O, 0, 0.8288025885, 1.885952763, −3.8908255334
H, 0, 0.9103884797, 2.8422322642, −4.0625558923
Al, 0, 0.7099242406, 0.7253193118, −0.3188124494

(4) $[Zn_5Al(OH_2)_{12}(OH)_{10}]^{3+}$
O, 0, −3.6249806189, −2.1080835455, 1.1740771833
H, 0, −3.7971795883, −2.732567288, 1.8980198534
Zn, 0, −1.8921683819, −1.9925238577, −0.2193733221
O, 0, −3.5019308278, −2.4837459767, −1.6370411453
H, 0, −3.5115694336, −2.8452804022, −2.5380252523
Zn, 0, 1.1846656063, −0.9485946154, −0.413627276
O, 0, −0.1796005124, −2.0663978986, −1.4822357228
H, 0, −0.1976868032, −2.0270635192, −2.4503514294
O, 0, 1.3030141259, −5.7345394892, 0.3903761001
H, 0, 2.2005553228, −6.0054934089, 0.6426200927
O, 0, 3.5523548405, −2.701101683, −2.1619723769
H, 0, 4.4836109139, −2.9562953568, −2.2639770799

Appendix A (*Continued*)

Zn, 0, 0.5713392915, −4.0099604134, −0.7223739755
O, 0, 2.0253070562, −2.7371526051, 0.0535955241
H, 0, 2.3552319576, −2.9083843134, 0.9481384248
O, 0, −0.7859888179, −5.7854564946, −1.3148371882
H, 0, −1.2221636416, −6.1448152113, −2.1040113721
O, 0, −1.194135417, −3.7946943566, 0.3521264575
H, 0, −1.1955433134, −4.0598055766, 1.2835480869
O, 0, 1.4760973127, −4.2413910833, −2.6153464961
H, 0, 1.6051502846, −5.1005695571, −3.0471409042
H, 0, 0.8367148969, −6.5273613439, 0.0704343493
H, 0, −3.926659608, −1.2337501175, 1.4705875269
H, 0, 2.3444896713, −3.7388082055, −2.6544159039
H, 0, 3.3223419285, −2.7566291125, −1.2018336724
H, 0, −4.3075318759, −2.7993206473, −1.1936705493
H, 0, −1.473785236, −5.4020738459, −0.7287474766
O, 0, −3.3217305445, 2.0189715159, 2.6898575093
O, 0, −2.4909375904, 0.0165101894, −0.3178756163
O, 0, −0.4657174168, −0.6197781958, 0.9503935663
H, 0, −4.2565374147, 2.1395269878, 2.9278063999
H, 0, −3.2244804058, 2.2580004141, 1.7421331759
H, 0, −3.1526389008, 0.3116300188, −0.9581909045
H, 0, −0.3069533272, −0.761892153, 1.8946638611
Zn, 0, 1.6835680832, 2.2831313677, −0.4184075037
O, 0, 0.2027790686, 1.9742563897, 1.3034515698
O, 0, 0.0766827815, 1.0377604909, −1.1562907929
O, 0, 2.5345899844, 0.4885225103, −0.21454844
O, 0, 0.8149354754, 4.1371375406, −0.3354351165
O, 0, 3.0415578595, 3.7281280113, 0.8388020463
H, 0, 0.608879794, 1.576154211, 2.085825727
H, 0, −0.2530783637, 1.0377951823, −2.0657808722
H, 0, 3.368158784, 0.3100366403, 0.2417923279
H, 0, 0.4877478648, 4.5311807787, −1.1573011726
H, 0, 3.996862512, 3.9016260286, 0.7742906537
H, 0, 2.5567584645, 4.4091849322, 0.3121632993
H, 0, 2.9402632619, 3.1915394799, −2.9450738655
O, 0, 2.7581179874, 2.4941555946, −2.294173202
H, 0, 3.3576655376, 1.7525696144, −2.4805286464
Zn, 0, −0.5047081552, 4.0077164038, 1.2498185046
O, 0, −1.9910048554, 2.6620355208, 0.3648582345
O, 0, −1.6568416332, 4.064344118, 3.04535957
O, 0, −1.5079166082, 5.8791536545, 0.9156022753
H, 0, −2.5753793861, 2.9353439862, −0.3580063909
H, 0, −1.1367552835, 4.0578401048, 3.8657530254
H, 0, −2.327293992, 3.3267968411, 3.1175768275
H, 0, −2.088557468, 6.1748423848, 1.637568821
H, 0, −1.2615190312, 6.6629057559, 0.3976163277
O, 0, 1.1109628195, 4.5225095409, 2.6704062969
H, 0, 1.2367217143, 5.3925797579, 3.0846428994
H, 0, 1.9843599235, 4.2561516232, 2.3060075767
Al, 0, −1.0889237562, 1.0440145217, 0.2624286089

(5) $[Zn_6Al(OH_2)_{12}(OH)_{12}]^{3+}$
O, 0, −1.5940779288, −2.8643443784, 2.0327199606
H, 0, −1.4657552285, −2.9491793418, 2.988055682
Zn, 0, 0.0615469133, −3.0995972425, 0.8343982062
O, 0, −0.9378250403, −4.448847192, −0.5733398316
H, 0, −0.7619440716, −5.3892711573, −0.7382049858
Zn, 0, 2.7830719573, −1.5303312521, 0.1825336481
O, 0, 1.9678243695, −3.3636133454, 0.0536547237
H, 0, 2.0428321044, −3.8115068284, −0.8020451062
O, 0, 4.4122967554, −1.5878897747, −1.6381833021
H, 0, 5.1240069288, −2.2247781404, −1.8216209745
O, 0, 4.2058919205, −2.2863632548, 1.6723396759
H, 0, 4.894797739, −1.8576685699, 2.205643274
O, 0, 1.0358607174, −4.4159108559, 2.2994820587
H, 0, 0.7543721504, −5.2262784947, 2.7551107655
H, 0, 4.7671702056, −0.8780682757, −1.0449454142
H, 0, −1.9137440258, −4.34432211, −0.4683451406
O, 0, −0.9953144502, −1.5787570915, −0.3032561732
O, 0, 1.0097116883, −1.088440002, 1.3168181415
H, 0, −1.2149890743, −1.8134811506, −1.2160801918
H, 0, 1.0427175023, −0.8680069977, 2.258713687
Zn, 0, 2.6057208513, 1.3653426811, −1.1259025891
O, 0, 1.0202187344, 1.6103134789, 0.4132164445
O, 0, 1.4246870921, −0.4217421834, −1.1539586029
O, 0, 3.8471357445, 0.2443964183, 0.0343635211
O, 0, 1.5229594382, 2.8425438388, −2.0694141934
O, 0, 3.4936885496, 3.5458338981, −0.6529493377

Appendix A (*Continued*)

H, 0, 1.2842480985, 1.8621122521, 1.3094297064
H, 0, 1.219161551, −0.8093397737, −2.0167509248
H, 0, 4.2701383386, 0.6765674063, 0.7898630444
H, 0, 1.3196431439, 2.7479921431, −3.0113797693
H, 0, 4.3868100001, 3.922481102, −0.7341697376
H, 0, 2.9872629318, 3.734744008, −1.4830264665
H, 0, 4.0456407939, 1.1224071991, −3.624671113
O, 0, 3.5035140979, 0.645341232, −2.9758951392
H, 0, 3.9270191131, −0.2301744917, −2.8191573241
Zn, 0, −0.0284095813, 3.0682964915, −0.7793084252
O, 0, −0.9755560025, 1.1051978326, −1.1492451302
O, 0, −1.5860109684, 4.1418416881, −2.2861972938
H, 0, −1.129014662, 0.8136000914, −2.0592313345
H, 0, −1.529700409, 4.94683668, −2.8290030467
H, 0, −1.9756617259, 4.3719716086, −1.4045109962
O, 0, 1.0874013775, 4.559596747, 0.37588984
H, 0, 0.918114912, 5.5098456719, 0.4808919801
H, 0, 2.0534917475, 4.4464714813, 0.2339779327
O, 0, −1.4192546867, 0.4152195509, 1.3293721264
Zn, 0, −2.6412376487, −1.3458188078, 1.1390362162
H, 0, −1.2250020866, 0.8072332981, 2.1927889342
O, 0, −4.1212012081, −1.3602075353, 2.7603639264
O, 0, −3.372099081, −3.5915550566, 0.3505903034
H, 0, −4.1212002297, −1.6732882152, 3.6793994322
H, 0, −4.2484251071, −4.0121437299, 0.3730572703
H, 0, −2.9275347003, −3.7407324786, 1.2251910325
H, 0, 4.3053766301, −3.2437034484, 1.7969368502
H, 0, 1.7881613452, −4.633768861, 1.7161301063
H, 0, −5.0132204524, −1.0295987572, 2.5694696146
H, 0, −4.2652799529, −0.4812458851, −0.6848454063
O, 0, −3.8748991582, −0.1232588575, 0.1261580502
Zn, 0, −2.7826931003, 1.6144520818, −0.058494915
O, 0, −4.3640326625, 2.2600536439, 1.3090323712
O, 0, −3.5021436892, 2.1263370223, −2.0820526952
O, 0, −1.8214334803, 3.4283376515, 0.1290848513
H, 0, −4.8509514207, 3.0973780969, 1.3834755116
H, 0, −5.0103684971, 1.5441875928, 1.1779957791
H, 0, −4.4147936256, 2.257413288, −2.386355347
H, 0, −2.9631647243, 2.8649386791, −2.4465498486
H, 0, −1.8318850154, 3.8498024227, 1.000716258
Al, 0, 0.0040731531, 0.0090451788, 0.0874944361

References

Aicken, A. M., Bell, I. S., Coveney, P. V., & Jones, W. (1997). Simulation of layered double hydroxide intercalates. *Advanced Materials*, *9*, 409–500.

Barriga, C., Jones, W., Malet, P., Rives, V., & Ulibarri, M. A. (1998). Synthesis and characterization of polyoxovanadate-pillared Zn–Al layered double hydroxides: An X-ray absorption and diffraction study. *Inorganic Chemistry*, *37*, 1812–1820.

Becke, A. D. (1988). Density-functional exchange-energy approximation with correct asymptotic behavior. *Physical Review A*, *38*, 3098–3100.

Becke, A. D. (1993). Density-functional thermochemistry. III. The role of exact exchange. *The Journal of Chemical Physics*, *98*, 5648–5652.

Bonnet, S., Forano, C., de Roy, A., Besse, J. P., Maillard, P., & Momenteau, M. (1996). Synthesis of hybrid organo-mineral materials: Anionic tetraphenylporphyrins in layered double hydroxides. *Chemistry of Materials*, *8*, 1962–1968.

Cavani, F., Trifirò, F., & Vaccari, A. (1991). Hydrotalcite-type anionic clays: Preparation, properties and applications. *Catalysis Today*, *11*(2), 173–301.

Chang, Z., Evans, D. G., Duan, X., Vial, C., Ghanbaja, J., Prevot, V., et al. (2005). Synthesis of [Zn–Al–CO_3] layered double hydroxides by a coprecipitation method under steady-state conditions. *Journal of Solid State Chemistry*, *178*, 2766–2777.

Chen, H., Zhang, F., Fu, S., & Duan, X. (2006). In situ microstructure control of oriented layered double hydroxide monolayer films with curved hexagonal crystals as superhydrophobic materials. *Advanced Materials*, *18*, 3089–3093.

Cho, S., Jung, S.-H., Jang, J.-W., Oh, E., & Lee, K.-H. (2008). Simultaneous synthesis of Al-doped ZnO nanoneedles and zinc aluminum hydroxides through use of a seed layer. *Crystal Growth & Design*, *8*, 4553–4558.

Choy, J.-H., Kwak, S.-Y., Park, J.-S., Jeong, Y.-J., & Portier, J. (1999). Intercalative nanohybrids of nucleoside monophosphates and DNA in layered metal hydroxide. *Journal of the American Chemical Society*, *121*, 1399–1400.

Darder, M., López-Blanco, M., Aranda, P., Leroux, F., & Ruiz-Hitzky, E. (2005). Bionanocomposites based on layered double hydroxides. *Chemistry of Materials*, *17*, 1969–1977.

del Arco, M., Rives, V., Trujillano, R., & Malet, P. (1996). Thermal behaviour of Zn–Cr layered double hydroxides with hydrotalcite-like structures containing carbonate or decavanadate. *Journal of Materials Chemistry*, *6*, 1419–1428.

Delgado, R. R., De Pauli, C. P., Carrasco, C. B., & Avena, M. J. (2008). Influence of M^{II}/M^{III} ratio in surface-charging behavior of Zn–Al layered double hydroxides. *Applied Clay Science*, *40*, 27–37.

Duan, X., Evans, D. G., & Mingos, D. M. P. (Eds.), (2006). *Structure and bonding*. Berlin: Springer.

Ennadi, A., Legrouri, A., de Roy, A., & Besse, J. P. (2000a). Shape and size determination for zinc–aluminium–chloride layered double hydroxide crystallites by analysis of X-ray diffraction line broadening. *Journal of Materials Chemistry*, *10*, 2337–2341.

Ennadi, A., Legrouri, A., de Roy, A., & Besse, J. P. (2000b). X-ray diffraction pattern simulation for thermally treated [Zn–Al–Cl] layered double hydroxide. *Journal of Solid State Chemistry*, *152*, 568–572.

Frisch, M. J., Trucks, G. W., Schlegel, H. B., Scuseria, G. E., Robb, M. A., Cheeseman, J. R., et al. (2003). *Gaussian 03, Revision B.04*. Pittsburgh, PA: Gaussian, Inc.

Greenwell, H. C., Jones, W., Coveney, P. V., & Stackhouse, S. (2006). On the application of computer simulation techniques to anionic and cationic clays: A materials chemistry perspective. *Journal of Materials Chemistry*, *16*, 708–723.

Greenwell, H. C., Stackhouse, S., Coveney, P. V., & Jones, W. (2003). A density functional theory study of catalytic trans-esterification by tert-butoxide MgAl anionic clays. *The Journal of Physical Chemistry B*, *107*, 3476–3485.

Gursky, J. A., Blough, S. D., Luna, C., Gomez, C., Luevano, A. N., & Gardner, E. A. (2006). Particle–particle interactions between layered double hydroxide nanoparticles. *Journal of the American Chemical Society*, *128*, 8376–8377.

Hay, P. J., & Wadt, W. R. (1985a). *Ab initio* effective core potentials for molecular calculations. Potentials for the transition metal atoms Sc to Hg. *Journal of Chemical Physics*, *82*, 270–283.

Hay, P. J., & Wadt, W. R. (1985b). *Ab initio* effective core potentials for molecular calculations. Potentials for K to Au including the outermost core orbitals. *Journal of Chemical Physics*, *82*, 299–310.

Hou, X., Kalinichev, A. G., & Kirkpatrick, R. J. (2002). Interlayer structure and dynamics of Cl–$LiAl_2$-layered double hydroxide: ^{35}Cl NMR observations and molecular dynamics modeling. *Chemistry of Materials*, *14*, 2078–2085.

Illaik, A., Taviot-Guého, C., Lavis, J., Commereuc, S., Verney, V., & Leroux, F. (2008). Unusual polystyrene nanocomposite structure using emulsifier-modified layered double hydroxide as nanofiller. *Chemistry of Materials*, *20*, 4854–4860.

Itoh, T., Shichi, T., Yui, T., Takahashi, H., Inui, Y., & Takagi, K. (2005). Reversible color changes in lamella hybrids of poly (diacetylenecarboxylates) incorporated in layered double hydroxide nanosheets. *The Journal of Physical Chemistry B*, *109*, 3199–3206.

Jaubertie, C., Holgado, M. J., Román, M. S. S., & Rives, V. (2006). Structural characterization and delamination of lactate-intercalated Zn, Al-layered double hydroxides. *Chemistry of Materials*, *18*, 3114–3121.

Lee, C., Yang, W., & Parr, R. G. (1988). Development of the Colle–Salvetti correlation-energy formula into a functional of the electron density. *Physical Review B*, *37*, 785–789.

Li, H., Ma, J., Evans, D. G., Zhou, T., Li, F., & Duan, X. (2006). Molecular dynamics modeling of the structures and binding energies of α-nickel hydroxides and nickel–aluminum layered double hydroxides containing various interlayer guest anions. *Chemistry of Materials*, *18*, 4405–4414.

Liu, J., Huang, X., Li, Y., Sulieman, K. M., He, X., & Sun, F. (2006). Facile and large-scale production of ZnO/Zn–Al layered double hydroxide hierarchical heterostructures. *The Journal of Physical Chemistry B*, *110*, 21865–21872.

Lombardo, G. M., Pappalardo, G. C., Costantino, F., Costantino, U., & Sisani, M. A. (2008). Thermal effects on mixed metal (Zn/Al) layered double hydroxides: Direct modeling of the X-ray powder diffraction line shape through molecular dynamics simulations. *Chemistry of Materials*, *20*, 5585–5592.

Lombardo, G. M., Pappalardo, G. C., Punzo, F., Costantino, F., Costantino, U., & Sisani, M. A. (2005). A novel integrated X-ray powder diffraction (XRPD) and molecular dynamics (MD) approach for modelling mixed-metal (Zn, Al) layered double hydroxides (LDHs). *European Journal of Inorganic Chemistry*, 5026–5034.

Mohanambe, L., & Vasudevan, S. (2005). Anionic clays containing anti-inflammatory drug molecules: Comparison of molecular dynamics simulation and measurements. *The Journal of Physical Chemistry B*, *109*, 15651–15658.

Oswald, H. R., & Asper, R. (1977). Bivalent metal hydroxides. In R. M. A. Lieth (Ed.), *Preparation and crystal growth of materials with layered structures* (pp. 71–140). Dordrecht: D. Reidel Publishing Company.

Petersson, G. A., & Al-Laham, M. A. (1991). A complete basis set model chemistry. II. Open-shell systems and the total energies of the first-row atoms. *The Journal of Chemical Physics*, *94*, 6081–6090.

Pisson, J., Morel, J. P., Morel-Desrosiers, N., Taviot-Guého, C., & Malfreyt, P. (2008). Molecular modeling of the structure and dynamics of the interlayer species of ZnAlCl layered double hydroxide. *The Journal of Physical Chemistry B*, *112*, 7856–7864.

Prevot, V., Forano, C., Besse, J. P., & Abraham, F. (1998). Syntheses and thermal and chemical behaviors of tartrate and succinate intercalated Zn_3Al and Zn_2Cr layered double hydroxides. *Inorganic Chemistry*, *37*, 4293–4301.

Pu, M., & Zhang, B. (2005). Theoretical study on the microstructures of hydrotalcite lamellae with Mg/Al ratio of two. *Materials Letters*, *59*, 3343–3347.

Refson, K., Park, S. H., & Sposito, G. (2003). Ab initio computational crystallography of 2:1 clay minerals. 1. Pyrophyllite-1Tc. *The Journal of Physical Chemistry B*, *107*, 13376–13383.

Rives, V. (Ed.). (2001). *Layered double hydroxides: Present and future*. New York: Nova Science Publishers Inc.

Rojas, R., de Pauli, C. P., Barriga, C., & Avena, M. J. (2008). Influence of M^{II}/M^{III} ratio in surface-charging behavior of Zn–Al layered double hydroxides. *Applied Clay Science*, *40*, 27–37.

Sainz-Diaz, C. I., Timon, V., Botella, V., & Hernandez-Laguna, A. (2000). Isomorphous substitution effect on the vibration frequencies of hydroxyl groups in

molecular cluster models of the clay octahedral sheet. *American Mineralogist*, *85*, 1038–1045.

Sato, H., Morita, A., Ono, K., Nakano, H., Wakabayashi, N., & Yamagishi, A. (2003). Templating effects on the mineralization of layered inorganic compounds: (1) Density functional calculations of the formation of single-layered magnesium hydroxide as a brucite model. *Langmuir*, *19*, 7120–7126.

Sauer, J. (1989). Molecular models in *ab initio* studies of solids and surfaces: From ionic crystals and semiconductors to catalysts. *Chemical Reviews*, *89*, 199–255.

Sauer, J., Ugliengo, P., Garonne, E., & Saunders, V. R. (1994). Theoretical study of van der Waals complexes at surface sites in comparison with the experiment. *Chemical Reviews*, *94*, 2095–2160.

Seftel, E. M., Popovici, E., Mertens, M., De Witte, K., van Tendeloo, G., Cool, P., et al. (2008). Zn–Al layered double hydroxides: Synthesis, characterization and photocatalytic application. *Microporous and Mesoporous Materials*, *113*, 296–304.

Sels, B. F., de Vos, D. E., & Jacobs, P. A. (2005). Bromide-assisted oxidation of substituted phenols with hydrogen peroxide to the corresponding *p*-quinol and *p*-quinol ethers over WO_4^{2-}-exchanged layered double hydroxides. *Angewandte Chemie, International Edition*, *44*, 310–313.

Shannon, R. D. (1976). Revised effective ionic radii and systematic studies of interatomic distances in halides and chalcogenides. *Acta Crystallographica*, *A32*, 751–767.

Thyveetil, M. A., Coveney, P. V., Greenwell, H. C., & Suter, J. L. (2008). Computer simulation study of the structural stability and materials properties of DNA-intercalated layered double hydroxides. *Journal of the American Chemical Society*, *130*, 4742–4756.

Trave, A., Selloni, A., Goursot, A., Tichit, D., & Weber, J. (2002). First principles study of the structure and chemistry of Mg-based hydrotalcite-like anionic clays. *The Journal of Physical Chemistry B*, *106*, 12291–12296.

Vial, S., Ghanbaja, J., & Forano, C. (2006). Precipitation of Zn_2Al LDH by urease enzyme. *Chemical Communications*, 290–292.

Wadt, W. R., & Hay, P. J. (1985). *Ab initio* effective core potentials for molecular calculations. Potentials for main group elements Na to Bi. *The Journal of Chemical Physics*, *82*, 284–298.

Yan, H., Lu, J., Wei, M., Ma, J., Li, H., He, J., et al. (2008). Theoretical study of the hexahydrated metal cations for the understanding of their template effects in the construction of layered double hydroxides. *Journal of Molecular Structure (Theochem)*, *866*, 34–45.

Yan, H., Wei, M., Ma, J., Li, F., Evans, D. G., & Duan, X. (2009). Theoretical study on the structural properties and relative stability of M(II)–Al layered double hydroxides based on a cluster model. *The Journal of Physical Chemistry A*, *113*, 6133–6141.

Yarger, M. S., Steinmiller, E. M. P., & Choi, K.-S. (2008). Electrochemical synthesis of Zn–Al layered double hydroxide (LDH) films. *Inorganic Chemistry*, *47*, 5859–5865.

Zhang, F., Zhao, L., Chen, H., Xu, S., Evans, D. G., & Duan, X. (2008). Corrosion resistance of superhydrophobic layered double hydroxide films on aluminum. *Angewandte Chemie, International Edition*, *47*, 2466–2469.

Zigan, F., & Rothbauer, R. (1967). Neutronenbeugungsmessungen am Brucit. *Neues Jahrbuch fiir Mineralogie Monatshefte*, 137–143.